ACS APPLIED MATERIALS & INTERFACES

Research Article

Cite This: ACS Appl. Mater. Interfaces 2018, 10, 12954−12959

www.acsami.org

Rational Design of Au@Pt Multibranched Nanostructures as Bifunctional Nanozymes

Jiangjiexing Wu,[†,‡] Kang Qin,[†] Dan Yuan,[†] Jun Tan,[†] Li Qin,[†] Xuejin Zhang,[†] and Hui Wei*[,†,‡,§]

[†]College of Engineering and Applied Sciences, Nanjing National Laboratory of Microstructures, [‡]State Key Laboratory of Coordination Chemistry, School of Chemistry and Chemical Engineering, and [§]State Key Laboratory of Analytical Chemistry for Life Science, School of Chemistry and Chemical Engineering, Collaborative Innovation Center of Chemistry for Life Sciences, Nanjing University, Nanjing 210093, China

Supporting Information

ABSTRACT: One of the current challenges in nanozyme-based nanotechnology is the utilization of multifunctionalities in one material. In this regard, Au@Pt nanoparticles (NPs) with excellent enzyme-mimicking activities due to the Pt shell and unique surface plasmon resonance features from the Au core have attracted enormous research interest. However, the unique surface plasmon resonance features from the Au core have not been widely utilized. The practical problem of the optical-damping nature of Pt hinders the research into the combination of Au@Pt NPs' enzyme-mimicking properties with their surface-enhanced Raman scattering (SERS) activities. Herein, we rationally tuned the Pt amount to achieve Au@Pt NPs with simultaneous plasmonic and enzyme-mimicking activities. The results showed that Au@Pt NPs with 2.5% Pt produced the highest Raman signal in 2 min, which benefited from the remarkably accelerated catalytic oxidation of 3,3′,5,5′-tetramethylbenzidine with the decorated Pt and strong electric field retained from the Au core for SERS. This study not only demonstrates the great promise of combining bimetallic nanomaterials' multiple functionalities but also provides rational guidelines to design high-performance nanozymes for potential biomedical applications.

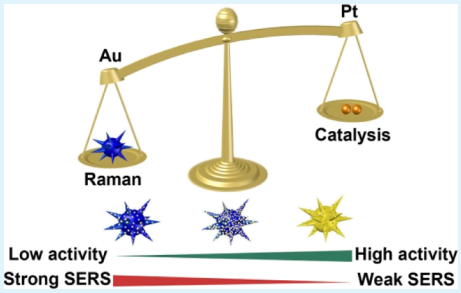

KEYWORDS: *Au@Pt nanoparticles, bifunctional nanozymes, core−shell structures, finite-difference time-domain (FDTD) simulation, surface-enhanced Raman scattering (SERS)*

INTRODUCTION

The functional nanomaterials such as metal oxide,[1−5] metal,[6−9] and others[10,11] with enzymelike characteristics, termed as nanozymes, are attracting immense attention in the field of artificial enzymes. Although remarkable achievements have been achieved over the past two decades, the functions of nanomaterials have not been fully utilized to construct multifunctional nanozymes.[12−14] For example, the plasmonic properties of noble metal nanoparticles (NPs) can enhance a probe molecule's Raman signal, thus providing a good sensitivity for detection.[15−17] Taking advantage of this, we recently developed surface-enhanced Raman scattering (SERS) active gold NPs (AuNPs) with peroxidase-mimicking properties for detection of glucose and lactate in live tissues.[18] However, the low catalytic activity of AuNPs costs half an hour for SERS detection, which in turn dramatically limits the future applications. To overcome this limitation, herein we have demonstrated a strategy to fabricate multifunctional Au@Pt nanozymes with significantly enhanced plasmonic and peroxidase-mimicking activities.

Recently, emerging research has focused on core−shell bimetallic Au@Pt nanostructures because of their synergistic properties and effective utilization of precious noble metals.[19−23] Au@Pt nanorods[24−31] and NPs[32−37] with enhanced catalytic activities have been used as peroxidase-, oxidase- and catalase-mimics in bioassays. However, the combination of Au@Pt NPs' enzyme-mimicking properties with their SERS activities is yet to be explored. This was probably because of the optical-damping effect of Pt, which made the enhancements for Raman and for catalytic activity apparently incompatible with each other. Lack of deep insights into such incompatibilities hampers the rational design of multifunctional Au@Pt nanozymes with simultaneous plasmonic and peroxidase-mimicking activities. To fill this gap, it is necessary to understand the effects of Pt on the catalytic and SERS properties of Au@Pt both experimentally and computationally, which will offer the groundwork for the rational design of high-performance nanozymes.

In this work, we prepared the Au@Pt NPs via a seed-mediated method with multibranched AuNPs as seeds. Various amounts of the Pt precursor led to Au@Pt NPs with different shapes and surface plasmon resonance (SPR) features. The prepared Au@Pt NPs acted not only as the peroxidase mimics for catalytically converting Raman-inactive reporters into active ones but also as the SERS-active substrates to enhance the activated reporters' Raman signals (Scheme 1). Then, we

Received: November 24, 2017
Accepted: March 26, 2018
Published: March 26, 2018

DOI: 10.1021/acsami.7b17945
ACS Appl. Mater. Interfaces 2018, 10, 12954−12959

Scheme 1. Rational Design of High-Performance Au@Pt NP Bifunctional Nanozymes by Controlling the Pt Amount

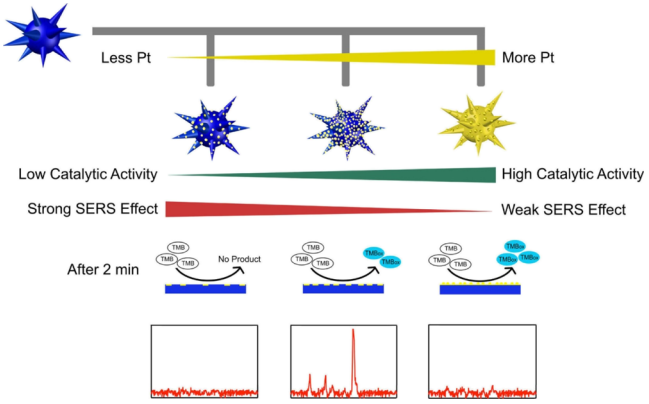

elucidated the role of Pt in modulating the catalytic and SERS activities of the Au@Pt NPs by kinetics studies and the finite difference time domain (FDTD) simulations. The Au@Pt NPs with an optimal Pt content for providing both high catalytic activity and good SERS activity were identified and fabricated, which were further employed for hydrogen peroxide sensing. The current study will not only provide deep insights into the effects of Pt on Au@Pt NPs' peroxidase-mimicking and SERS activities but also boost the development of rational-designed multifunctional nanozymes for potential biomedical applications.

EXPERIMENTAL SECTION

Chemicals and Materials. Hydrogen tetrachloroaurate(III) hydrate ($HAuCl_4 \cdot xH_2O$, Au ≥ 47.5%, Aladdin), silver nitrate ($AgNO_3$, 99.8%, Sinopharm Chemical Reagent Co.), L-ascorbic acid (AA, ≥99.0%, Sigma-Aldrich), chloroplatinic acid hexahydrate(IV) ($H_2PtCl_6 \cdot 6H_2O$, Pt ≥ 37.5%, Aladdin), 3,3′,5,5′-tetramethylbenzidine dihydrochloride (TMB, Aladdin), hydrogen peroxide (H_2O_2, Sinopharm Chemical Reagent Co.), and sodium acetate (NaOAc, Nanjing Chemical Co.) were used without further purification. Deionized water (18.2 MΩ) was used in all procedures.

Synthesis of Multibranched Gold Nanostructures. Multibranched AuNPs were synthesized as follows.[38] Aqueous $HAuCl_4$ solution (20 μL, 10 mM) was first mixed with 1 mL of water, and then 3 μL of 10 mM aqueous $AgNO_3$ solution was added. After the solutions were thoroughly mixed, 4 μL of 100 mM freshly prepared AA was quickly added and vigorously shaken for 20 s at room temperature. After centrifugation at a speed of 4800 rpm for 10 min, the AuNPs were redispersed in 1 mL of water for further use.

Synthesis of Au@Pt Bimetallic Nanostructures. Au@Pt NPs were prepared through a seed-mediated method. The as-prepared AuNPs solution was used as the seed. H_2PtCl_6 solution (5 μL; 0.1, 1, and 10 mM separately) was added to 1 mL of seed solution, and the solution was vortexed. Next, 4 μL of 100 mM AA was introduced to initiate the reduction reaction. After the solutions were thoroughly mixed, they were kept at room temperature for 1 h.

Au@Pt NPs for Catalytic Oxidation of TMB and for SERS Measurements. For a typical test, 400 μL of 0.4 nM Au@Pt NPs was added into 50 mM NaOAc buffer (pH = 4.5) containing H_2O_2 (4 μL, 20 mM) and TMB (8 μL, 1 mM). The final volume of the mixed solution was adjusted to 0.8 mL with the buffer. The mixture was then incubated at room temperature for 2 min and used for SERS measurements.

Kinetics Analysis of AuNPs and Au@Pt NPs. The kinetics experiments for the catalytic oxidation of TMB with H_2O_2 were carried out at room temperature in 50 mM NaOAc buffer solution (pH 4.5) containing 0.2 nM AuNPs (or Au@Pt NPs), 16 mM H_2O_2, and different concentrations of TMB. The absorbance of the reaction solution at 652 nm was immediately measured as a function of time using a spectrophotometer with a 1.0 cm quartz cell for 5 min. The Michaelis constant was calculated using a double reciprocal plot: $1/v = K_m/V_{max}\ (1/[S] + 1/K_m)$, where v is the initial velocity, V_{max} is the maximal reaction velocity, [S] is the substrate concentration, and K_m is the Michaelis constant.

Detection of H_2O_2 with Au@$Pt_{2.5\%}$ NPs. Typically, 10 μL of H_2O_2 with different concentrations (final concentration was 0.5−30 μM) was added into the mixture containing 50 mM NaOAc buffer (pH = 4.5), TMB (8 μL, 0.1 mM), and Au@$Pt_{2.5\%}$ (400 μL, 0.4 nM). The mixture was then incubated at room temperature for 2 min and used for SERS measurements.

Theoretical Simulation. The simulations were performed by using the FDTD software (Lumerical FDTD Solutions). During the calculations, an X-polarized light with a 633 nm wavelength was launched into a box containing the target nanostructure to simulate a propagating plane wave interacting with the nanostructure. The refractive index of the surrounding medium was water, set as 1.33. The multibranched AuNP was modeled as a circle core capped with protruding tips on the surface. The morphology and size of the AuNPs agreed qualitatively with the one inferred from the transmission electron microscopy (TEM) images. According to the elemental mapping results, the Pt shell was modeled by adding different amounts of circles onto the surface of Au.

Instrumentation and Characterization. Ultraviolet−visible−near-infrared (UV−vis−NIR) absorption spectra were collected on a Shimadzu UV-3600 plus spectrophotometer with a 1.0 cm quartz cell under ambient conditions. TEM imaging was performed with a FEI Tecnai F20 microscope at an acceleration voltage of 200 kV. Energy-dispersive X-ray spectroscopy (EDS) elemental mapping and line-scanning in the scanning TEM (STEM) mode were carried out on a double aberration-corrected Titan cubed G2 60-300 S/TEM equipped with Super-XTM Technology. Raman spectra were obtained on an Advantage Raman spectrometer (DeltaNu) with a 633 nm laser and 2 s integration time.

RESULTS AND DISCUSSION

Au@Pt NPs were prepared via a seed-mediated method with various amounts of the Pt precursor. The Au multibranched nanostructures as seeds (~80 nm, Figures 1, S1, and S2) were first synthesized. These multibranched AuNPs were ideal SERS substrates, as the large core size, cone-shaped branches, and the gaps between the neighboring branches would ensure a high SERS activity.[38] Before growing Pt on the AuNPs, the amount of Pt to form one layer was estimated to be 2×10^4 nM (Figure S3). The growth of Pt on AuNPs is known to prefer the Volmer−Weber mode because of the higher surface energy of Pt than that of Au;[21,25,39] thus, more Pt atoms than the estimated value would be required to form the Pt shell. Here, 5×10^4 nM Pt was chosen to form an entirely covered Pt shell (designated as Au@$Pt_{25\%}$, 25% for the Pt/Au molar ratio of 0.25). To study the effect of Pt content on the catalytic and SERS properties of AuNPs, less amount of Pt (i.e., 5×10^3 and 5×10^2 nM) was chosen to fabricate Au@Pt with an incomplete Pt coverage (designated as Au@$Pt_{2.5\%}$ and Au@$Pt_{0.25\%}$, respectively). Typical TEM images in Figure 1 showed that there were nearly no morphological changes for Au@$Pt_{0.25\%}$ and Au@$Pt_{2.5\%}$ compared to the AuNPs. By contrast, for Au@$Pt_{25\%}$, well-distributed Pt nanodots (diameter ca. 2 nm) were clearly observed on the AuNP core.

Such structural transformations were accompanied by the corresponding changes in their optical properties. The color of the multibranched AuNPs aqueous solution was blue, which gradually changed to gray with the increase of the Pt precursor amount (Figure 2 inset). As shown in Figure 2, the multibranched AuNPs displayed two peaks of transverse and

DOI: 10.1021/acsami.7b17945
ACS Appl. Mater. Interfaces 2018, 10, 12954−12959

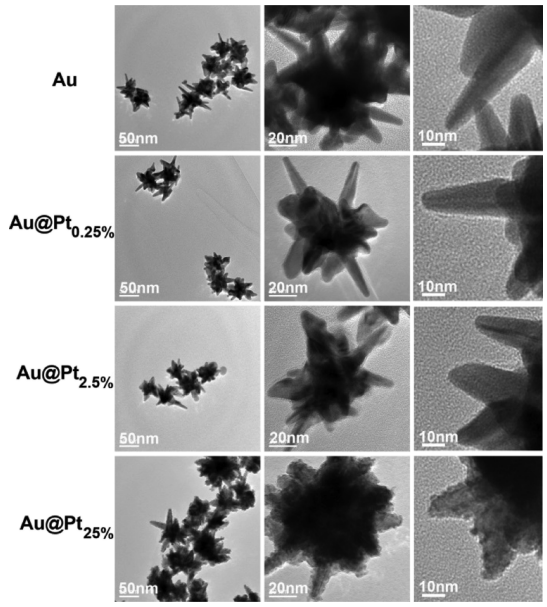

Figure 1. Bright-field TEM images of AuNPs and Au@Pt NPs with different Pt contents. Left panel shows the overall multibranched shapes and good uniformity of the samples. Middle and right panels are the TEM images of an individual NP and branches at a higher magnification.

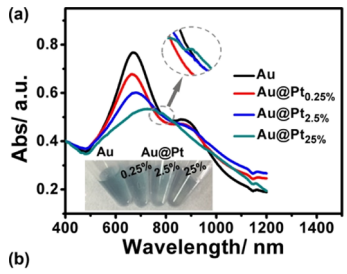

Absorption peaks of Au@Pt multibranched nanostructures/ nm

Au	670	870
$Au@Pt_{0.25\%}$	670	870
$Au@Pt_{2.5\%}$	670	870
$Au@Pt_{25\%}$	728	782

Figure 2. (a) UV−vis−NIR absorption spectra of AuNPs and Au@Pt NPs. Inset: corresponding image of AuNPs and Au@Pt NPs. Circle: magnification of the absorption peak at 782 nm for $Au@Pt_{25\%}$. (b) Absorption peaks of AuNPs and Au@Pt multibranched nanostructures.

longitudinal mode SPR bands at 670 and 870 nm, respectively. It is known that the position of the two bands is dependent on the size of the core and the length of the branches.[38] For $Au@Pt_{0.25\%}$ and $Au@Pt_{2.5\%}$, the growth of Pt only decreased the intensity of the two peaks at 670 and 870 nm but did not induce any obvious SPR band shift, which was consistent with the TEM results, as no shape changes were observed in Figure 1. Different from $Au@Pt_{0.25\%}$ and $Au@Pt_{2.5\%}$, $Au@Pt_{25\%}$ presented only one major transverse peak at 728 nm, and the longitudinal plasmon band blue-shifted to 782 nm as a small shoulder. This was easy to understand given the fact that the obvious growth of Pt islands on AuNPs made the sphere core bigger and the branches thicker and shorter; thus the transverse SPR band red-shifted and the longitudinal one blue-shifted. The larger shift of the longitudinal SPR band was due to the more polarizable and more sensitive properties of the longitudinal plasmon than that of the transverse one. For all three Au@Pt NPs, although the growth of Pt decreased the intensities of SPR bands, the SPR peaks were still retained, providing these structures with electromagnetic fields for SERS.[40]

To further study the elemental compositions of the core and shell for each NP obtained, we performed STEM−EDS mapping and line scan analysis. The elemental mapping (Figure 3) revealed that the Au nanostructure clearly resided at the core

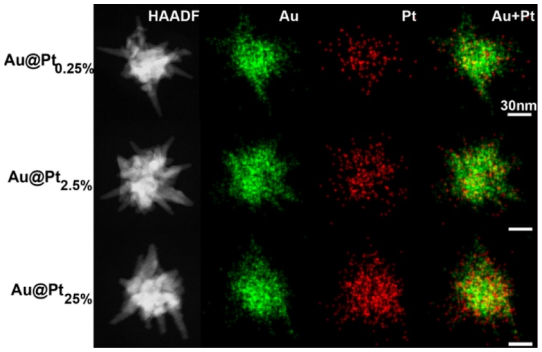

Figure 3. High-angle annular dark field STEM images of Au@Pt NPs with different Pt contents and their corresponding elemental mapping.

of each Au@Pt NP, whereas the Pt distributed outside as the shell. The line-scanning results (Figure S4) also demonstrated the core−shell structures after growing Pt on the AuNPs, with a bimodal Pt distribution at the edge and a higher concentration of Au at the center of the NP. Furthermore, when comparing the intensity of Pt distribution between the sphere core and branches (Figure 3), it was found that more Pt would deposit on the sphere core, especially for $Au@Pt_{0.25\%}$ and $Au@Pt_{2.5\%}$. This was consistent with the UV−vis−NIR results, as the intensity of the SPR peak at 670 nm decreased much more than the one at 870 nm.

The simultaneous peroxidase-mimicking and SERS activities of the Au@Pt NPs were then evaluated. Pt would catalyze the oxidation of TMB with H_2O_2 into oxidized TMB (TMB_{ox}), which has an absorbance peak at 650 nm and thus could be in resonance with a 633 nm laser excitation.[41] The Au of the Au@Pt NPs would ensure SERS enhancement, thus providing strong SERS signals. After TMB, H_2O_2 and the NPs were incubated together for 2 min (Figure S5) at room temperature, all solutions were colorless (Figure S6), which could not be distinguished by the naked eye or even by absorption spectroscopy. By contrast, significantly different SERS spectra were obtained for the NPs (Figure 4). The highest signal at 1605 cm^{-1} was chosen for the following quantitative study. The $Au@Pt_{2.5\%}$ showed the highest signal of 2582 at 1605 cm^{-1}, whereas the AuNPs and $Au@Pt_{0.25\%}$ exhibited almost no signals, and $Au@Pt_{25\%}$ gave a much lower signal of 280.

It is widely accepted that the catalytic activities would be enhanced by growing Pt onto AuNPs.[25,36,37,42] Unexpectedly, the SERS signals of $Au@Pt_{25\%}$ shown in Figure 4 decreased when compared with the signals of $Au@Pt_{2.5\%}$. To understand this unexpected tendency, FDTD simulations were performed to reveal how different Pt contents would affect the electromagnetic field of AuNPs. The multibranched AuNP was modeled as a solid core with protruding tips. The morphology and size of the AuNP as well as the Pt distribution

DOI: 10.1021/acsami.7b17945
ACS Appl. Mater. Interfaces 2018, 10, 12954−12959

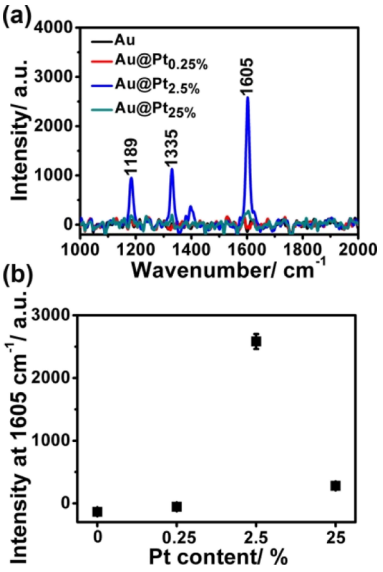

Figure 4. (a) SERS spectra of the samples containing 0.01 mM TMB, 0.1 mM H_2O_2, and 0.2 nM AuNPs or Au@Pt NPs (0.25%, 2.5%, and 25% Pt) in 50 mM NaOAc (pH 4.5) after 2 min of incubation at room temperature using 633 nm laser excitation and 2 s integration time. (b) Plots of Raman intensity of oxidized TMB at 1605 cm^{-1} vs Pt content. The error bars indicate standard deviations of three independent measurements.

agreed qualitatively with the ones inferred from the above TEM and EDS images. The calculated results showed that AuNPs gave the strongest electric field with the locations at the tip of the branches and in the gap region between the core surface and the branch. The growth of Pt would damp the electric field of AuNPs a lot (Figure 5). Despite 0.25%, 2.5%, and 25% Pt all

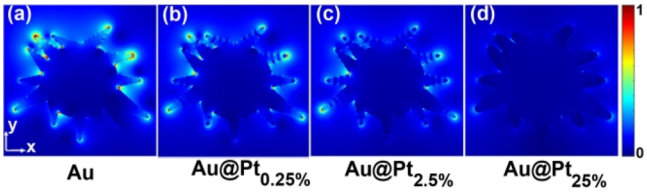

Figure 5. Simulated electric-field distributions of AuNP (a) and Au@Pt NPs with increased Pt amount (b–d) under X-polarized illumination at a wavelength of 633 nm. The morphologies, size, and Pt distribution were obtained from TEM and elemental mapping results.

decreasing the electric field, the Raman signals did not show a monotonic decrease tendency either. Therefore, the obtained Raman signals should be the balanced results of catalysis and SERS.

To clearly elucidate the two roles of Pt on Au, we first compared the AuNPs and Au@Pt NPs. Figure 4 showed that except $Au@Pt_{0.25\%}$, the other two Au@Pt NPs (i.e., $Au@Pt_{2.5\%}$ and $Au@Pt_{25\%}$) exhibited obviously higher Raman signals than of AuNPs, suggesting that the high catalytic activity of Pt was dominant for producing high Raman signals although the electric field was damped. The result of $Au@Pt_{0.25\%}$ was interesting as it showed negligible signal at 2 min, indicating that nearly no TMB_{ox} was produced within 2 min. The electronic effect between the core and shell atoms may provide some insights into the mechanism.[43−45] It is known that the catalytic oxidation of TMB with H_2O_2 first needed the adsorption of both the reactants and then activated them for further reactions. H_2O_2 is known to be easily adsorbed onto the surface of Pt and activated to oxidize TMB into TMB_{ox}.[24] On the other hand, the adsorption of TMB to the Au surface would be promoted in the Au@Pt system. In Au@Pt NPs, subtle electronic charges transferred from Pt to Au because of their different electronegativity,[44,46−49] which would lead to an increase in the electron density on the Au surface (Figure S7). Meanwhile, the acidic condition made the TMB partially protonated and positively charged. As such, the electrostatic interaction between the Au and TMB would facilitate the adsorption of TMB. Benefited from the promoted adsorption of TMB and the enhanced ability to activate H_2O_2, the TMB_{ox} would be generated and give SERS signals within 2 min (Figure S8). But when the amount of Pt was too little to make the Au surface negative enough, the adsorption and catalytic oxidation of TMB would consequently be slow, just like $Au@Pt_{0.25\%}$, which was consistent with the kinetic studies (Figure S9 and Table S1). To further confirm the role of the electronic effect, we studied another two Pt contents. As shown in Figure S10, $Au@Pt_{0.025\%}$ showed no signal, whereas $Au@Pt_{1.25\%}$ gave a signal of 206 at 1605 cm^{-1}, suggesting that the more the electrons transferred, the more TMB adsorbed, and thus the catalytic oxidation of TMB was promoted. Furthermore, after 2 h, these initially low signals all increased as high as ∼3000, which further demonstrated the hypothesis. The AuNPs presented the highest signal of 4700 because of the strongest electric field enhancement (Figure S11).

Next, we investigated the Au@Pt NPs with different Pt amounts. Despite $Au@Pt_{1.25\%}$, $Au@Pt_{2.5\%}$ and $Au@Pt_{25\%}$ all exhibiting SERS signals, the intensities were different. For Pt less than 2.5%, the above study has shown that the different signal intensities were attributed to the rate of the reaction, whereas for Pt more than 2.5%, the weakened signal was due to the decayed plasmon field according to the simulation results. Applying this explanation to the $Au@Pt_{12.5\%}$ system with a medium amount of Pt between 2.5% and 25%, it was predicted to have a Raman signal between 2500 and 280. The measurement (Figure S10) indeed presented a signal of 656 at 1605 cm^{-1}, consistent with the prediction.

Finally, $Au@Pt_{2.5\%}$, with both high enzyme-mimicking catalytic activities and SERS properties, was chosen for developing a H_2O_2 assay. It was facile to determine H_2O_2 by this reaction because the catalytic activity and the produced SERS intensity were H_2O_2 concentration-dependent. As seen in Figure S12, the Raman intensity of TMB_{ox} catalyzed by $Au@Pt_{2.5\%}$ increased with increasing H_2O_2 concentrations. A good linear relationship (r = 0.99) was also obtained between the SERS intensities at 1605 cm^{-1} versus the H_2O_2 concentrations from 1 to 30 μM. The current system showed unique advantages with respect to previously reported methods. As shown in Table S2, the combination of AuNPs' SERS activities and PtNPs' high catalytic activities shortened the assay time and improved the sensitivity by 1−2 orders of magnitude.

CONCLUSIONS

In conclusion, we have investigated the effects of Pt contents on the peroxidase-mimicking and SERS activities of multibranched AuNPs. The Au@Pt NPs were synthesized through a seed-mediated method to provide monodispersed bimetallic NPs. The observation through TEM and elemental mapping demonstrated that the Au@Pt NPs formed the core−shell structures. The Raman and FDTD studies indicated that less Pt

DOI: 10.1021/acsami.7b17945
ACS Appl. Mater. Interfaces 2018, 10, 12954−12959

on Au exhibited lower signals, caused by weak electric effect, and the same phenomena for more Pt was attributed to the decreased electric field. Only Au@$Pt_{2.5\%}$, good peroxidase-like nanozyme, gave the highest Raman signal in 2 min. These insights have enriched our understanding of the effect of Pt contents on Au. It will provide a reliable guideline to rationally design high-performance nanozymes with sensitive SERS properties for potential biomedical applications.

■ ASSOCIATED CONTENT

Supporting Information

The Supporting Information is available free of charge on the ACS Publications website at DOI: 10.1021/acsami.7b17945.

Additional supporting figures of TEM measurements, EDS measurements, SERS measurements, kinetics studies, and possible mechanism scheme (PDF)

■ AUTHOR INFORMATION

Corresponding Author

*E-mail: weihui@nju.edu.cn. Phone: +86-25-83593272. Fax: +86-25-83594648. Web: weilab.nju.edu.cn.

ORCID

Hui Wei: 0000-0003-0870-7142

Notes

The authors declare no competing financial interest.

■ ACKNOWLEDGMENTS

This work was supported by the National Natural Science Foundation of China (21722503 and 21405081), the Natural Science Foundation of Jiangsu Province (BK20160615), 973 Program (2015CB659400), the PAPD program, the Shuangchuang Program of Jiangsu Province, the Six Talents Summit Program of Jiangsu Province, Open Funds of the State Key Laboratory of Coordination Chemistry (SKLCC1619 and SKLCC1819), Open Funds of the State Key Laboratory of Analytical Chemistry for Life Science (SKLACLS1704), the China Postdoctoral Science Foundation (2016M590437), Fundamental Research Funds for the Central Universities (021314380046), and the Thousand Talents Program for Young Researchers. We thank Peng Wang, Jiamei Song, and Xuhao Hong for help with TEM.

■ REFERENCES

(1) Gao, L.; Zhuang, J.; Nie, L.; Zhang, J.; Zhang, Y.; Gu, N.; Wang, T.; Feng, J.; Yang, D.; Perrett, S.; Yan, X. Intrinsic Peroxidase-Like Activity of Ferromagnetic Nanoparticles. *Nat. Nanotechnol.* **2007**, *2*, 577−583.

(2) Fan, K.; Wang, H.; Xi, J.; Liu, Q.; Meng, X.; Duan, D.; Gao, L.; Yan, X. Optimization of Fe_3O_4 Nanozyme Activity via Single Amino Acid Modification Mimicking an Enzyme Active Site. *Chem. Commun.* **2017**, *53*, 424−427.

(3) Zhang, Z.; Zhang, X.; Liu, B.; Liu, J. Molecular Imprinting on Inorganic Nanozymes for Hundred-fold Enzyme Specificity. *J. Am. Chem. Soc.* **2017**, *139*, 5412−5419.

(4) Wang, Q.; Zhang, X.; Huang, L.; Zhang, Z.; Dong, S. One-Pot Synthesis of Fe_3O_4 Nanoparticle Loaded 3D Porous Graphene Nanocomposites with Enhanced Nanozyme Activity for Glucose Detection. *ACS Appl. Mater. Interfaces* **2017**, *9*, 7465−7471.

(5) Liu, B.; Sun, Z.; Huang, P.-J. J.; Liu, J. Hydrogen Peroxide Displacing DNA from Nanoceria: Mechanism and Detection of Glucose in Serum. *J. Am. Chem. Soc.* **2015**, *137*, 1290−1295.

(6) Lin, Y.; Ren, J.; Qu, X. Nano-Gold as Artificial Enzymes: Hidden Talents. *Adv. Mater.* **2014**, *26*, 4200−4217.

(7) Deng, H.-H.; Lin, X.-L.; Liu, Y.-H.; Li, K.-L.; Zhuang, Q.-Q.; Peng, H.-P.; Liu, A.-L.; Xia, X.-H.; Chen, W. Chitosan-Stabilized Platinum Nanoparticles as Effective Oxidase Mimics for Colorimetric Detection of Acid Phosphatase. *Nanoscale* **2017**, *9*, 10292−10300.

(8) Li, H.; Liu, H.; Zhang, J.; Cheng, Y.; Zhang, C.; Fei, X.; Xian, Y. Platinum Nanoparticle Encapsulated Metal-Organic Frameworks for Colorimetric Measurement and Facile Removal of Mercury(II). *ACS Appl. Mater. Interfaces* **2017**, *9*, 40716−40725.

(9) Liang, H.; Lin, F.; Zhang, Z.; Liu, B.; Jiang, S.; Yuan, Q.; Liu, J. Multicopper Laccase Mimicking Nanozymes with Nucleotides as Ligands. *ACS Appl. Mater. Interfaces* **2017**, *9*, 1352−1360.

(10) Lu, C.; Liu, X.; Li, Y.; Yu, F.; Tang, L.; Hu, Y.; Ying, Y. Multifunctional Janus Hematite−Silica Nanoparticles: Mimicking Peroxidase-Like Activity and Sensitive Colorimetric Detection of Glucose. *ACS Appl. Mater. Interfaces* **2015**, *7*, 15395−15402.

(11) Li, Y.-Z.; Li, T.-T.; Chen, W.; Song, Y.-Y. Co_4N Nanowires: Noble-Metal-Free Peroxidase Mimetic with Excellent Salt- and Temperature-Resistant Abilities. *ACS Appl. Mater. Interfaces* **2017**, *9*, 29881−29888.

(12) Wei, H.; Wang, E. Nanomaterials with Enzyme-Like Characteristics (Nanozymes): Next-Generation Artificial Enzymes. *Chem. Soc. Rev.* **2013**, *42*, 6060−6093.

(13) Wang, X.; Hu, Y.; Wei, H. Nanozymes in Bionanotechnology: From Sensing to Therapeutics and Beyond. *Inorg. Chem. Front.* **2016**, *3*, 41−60.

(14) Liu, B.; Liu, J. Surface Modification of Nanozymes. *Nano Res.* **2017**, *10*, 1125−1148.

(15) Qian, X.; Emory, S. R.; Nie, S. Anchoring Molecular Chromophores to Colloidal Gold Nanocrystals: Surface-Enhanced Raman Evidence for Strong Electronic Coupling and Irreversible Structural Locking. *J. Am. Chem. Soc.* **2012**, *134*, 2000−2003.

(16) Wang, Y.; Wee, E. J. H.; Trau, M. Accurate and Sensitive Total Genomic DNA Methylation Analysis from Sub-Nanogram Input with Embedded SERS Nanotags. *Chem. Commun.* **2016**, *52*, 3560−3563.

(17) Guo, Y.; Wang, H.; Ma, X.; Jin, J.; Ji, W.; Wang, X.; Song, W.; Zhao, B.; He, C. Fabrication of Ag−Cu_2O/Reduced Graphene Oxide Nanocomposites as Surface-Enhanced Raman Scattering Substrates for in Situ Monitoring of Peroxidase-Like Catalytic Reaction and Biosensing. *ACS Appl. Mater. Interfaces* **2017**, *9*, 19074−19081.

(18) Hu, Y.; Cheng, H.; Zhao, X.; Wu, J.; Muhammad, F.; Lin, S.; He, J.; Zhou, L.; Zhang, C.; Deng, Y.; Wang, P.; Zhou, Z.; Nie, S.; Wei, H. Surface-Enhanced Raman Scattering Active Gold Nanoparticles with Enzyme-Mimicking Activities for Measuring Glucose and Lactate in Living Tissues. *ACS Nano* **2017**, *11*, 5558−5566.

(19) Iyyamperumal, R.; Zhang, L.; Henkelman, G.; Crooks, R. M. Efficient Electrocatalytic Oxidation of Formic Acid Using Au@Pt Dendrimer-Encapsulated Nanoparticles. *J. Am. Chem. Soc.* **2013**, *135*, 5521−5524.

(20) Bian, T.; Zhang, H.; Jiang, Y.; Jin, C.; Wu, J.; Yang, H.; Yang, D. Epitaxial Growth of Twinned Au−Pt Core−Shell Star-Shaped Decahedra as Highly Durable Electrocatalysts. *Nano Lett.* **2015**, *15*, 7808−7815.

(21) Zhou, S.; McIlwrath, K.; Jackson, G.; Eichhorn, B. Enhanced CO Tolerance for Hydrogen Activation in Au−Pt Dendritic Heteroaggregate Nanostructures. *J. Am. Chem. Soc.* **2006**, *128*, 1780−1781.

(22) Tian, Z.-Q.; Ren, B.; Li, J.-F.; Yang, Z.-L. Expanding Generality of Surface-Enhanced Raman Spectroscopy with Borrowing SERS Activity Strategy. *Chem. Commun.* **2007**, 3514−3534.

(23) Zhou, W.; Ding, J.; Liu, J. A Platinum Shell for Ultraslow Ligand Exchange: Unmodified DNA Adsorbing More Stably on Platinum than Thiol and Dithiol on Gold. *Chem. Commun.* **2015**, *51*, 12084−12087.

(24) Li, J.; Liu, W.; Wu, X.; Gao, X. Mechanism of pH-Switchable Peroxidase and Catalase-Like Activities of Gold, Silver, Platinum and Palladium. *Biomaterials* **2015**, *48*, 37−44.

(25) He, W.; Liu, Y.; Yuan, J.; Yin, J.-J.; Wu, X.; Hu, X.; Zhang, K.; Liu, J.; Chen, C.; Ji, Y.; Guo, Y. Au@Pt Nanostructures as Oxidase and Peroxidase Mimetics for Use in Immunoassays. *Biomaterials* **2011**, *32*, 1139−1147.

(26) Liu, J.; Hu, X.; Hou, S.; Wen, T.; Liu, W.; Zhu, X.; Yin, J.-J.; Wu, X. Au@Pt Core/Shell Nanorods with Peroxidase- and Ascorbate Oxidase-Like Activities for Improved Detection of Glucose. *Sens. Actuators, B* **2012**, *166*, 708−714.
(27) Zhou, Y.-T.; He, W.; Wamer, W. G.; Hu, X.; Wu, X.; Lo, Y. M.; Yin, J.-J. Enzyme-Mimetic Effects of Gold@Platinum Nanorods on the Antioxidant Activity of Ascorbic Acid. *Nanoscale* **2013**, *5*, 1583−1591.
(28) Liu, J.; Hu, X.; Hou, S.; Wen, T.; Liu, W.; Zhu, X.; Wu, X. Screening of Inhibitors for Oxidase Mimics of Au@Pt Nanorods by Catalytic Oxidation of OPD. *Chem. Commun.* **2011**, *47*, 10981−10983.
(29) Feng, X.; Li, X.; Shi, H.; Huang, H.; Wu, X.; Song, W. Highly Accessible Pt Nanodots Homogeneously Decorated on Au Nanorods Surface for Sensing. *Anal. Chim. Acta* **2014**, *852*, 37−44.
(30) Lee, J.-W.; Yoon, S.; Lo, Y. M.; Wu, H.; Lee, S.-Y.; Moon, B. Intrinsic Polyphenol Oxidase-Like Activity of Gold@Platinum Nanoparticles. *RSC Adv.* **2015**, *5*, 63757−63764.
(31) Liu, J.; Jiang, X.; Wang, L.; Hu, Z.; Wen, T.; Liu, W.; Yin, J.; Chen, C.; Wu, X. Ferroxidase-Like Activity of Au Nanorod/Pt Nanodot Structures and Implications for Cellular Oxidative Stress. *Nano Res.* **2015**, *8*, 4024−4037.
(32) Fu, Q.; Wu, Z.; Du, D.; Zhu, C.; Lin, Y.; Tang, Y. Versatile Barometer Biosensor Based on Au@Pt Core/Shell Nanoparticle Probe. *ACS Sens.* **2017**, *2*, 789−795.
(33) Gao, Z.; Xu, M.; Lu, M.; Chen, G.; Tang, D. Urchin-Like (Gold Core)@(Platinum Shell) Nanohybrids: A Highly Efficient Peroxidase-Mimetic System for In Situ Amplified Colorimetric Immunoassay. *Biosens. Bioelectron.* **2015**, *70*, 194−201.
(34) Pan, N.; Zhu, Y.; Wu, L.-L.; Xie, Z.-J.; Xue, F.; Peng, C.-F. Highly Sensitive Colorimetric Detection of Copper Ions based on Regulating the Peroxidase-Like Activity of Au@Pt Nanohybrids. *Anal. Methods* **2016**, *8*, 7531−7536.
(35) Pan, N.; Li-Ying, W.; Wu, L.-L.; Peng, C.-F.; Xie, Z.-J. Colorimetric Determination of Cysteine by Exploiting Its Inhibitory Action on the Peroxidase-Like Activity of Au@Pt Core-Shell Nanohybrids. *Microchim. Acta* **2017**, *184*, 65−72.
(36) Zhu, Z.; Guan, Z.; Jia, S.; Lei, Z.; Lin, S.; Zhang, H.; Ma, Y.; Tian, Z.-Q.; Yang, C. J. Au@Pt Nanoparticle Encapsulated Target-Responsive Hydrogel with Volumetric Bar-Chart Chip Readout for Quantitative Point-of-Care Testing. *Angew. Chem., Int. Ed.* **2014**, *53*, 12503−12507.
(37) Gao, Z.; Ye, H.; Tang, D.; Tao, J.; Habibi, S.; Minerick, A.; Tang, D.; Xia, X. Platinum-Decorated Gold Nanoparticles with Dual Functionalities for Ultrasensitive Colorimetric in Vitro Diagnostics. *Nano Lett.* **2017**, *17*, 5572−5579.
(38) Cheng, L.-C.; Huang, J.-H.; Chen, H. M.; Lai, T.-C.; Yang, K.-Y.; Liu, R.-S.; Hsiao, M.; Chen, C.-H.; Her, L.-J.; Tsai, D. P. Seedless, Silver-Induced Synthesis of Star-Shaped Gold/Silver Bimetallic Nanoparticles as High Efficiency Photothermal Therapy Reagent. *J. Mater. Chem.* **2012**, *22*, 2244−2253.
(39) Ataee-Esfahani, H.; Wang, L.; Nemoto, Y.; Yamauchi, Y. Synthesis of Bimetallic Au@Pt Nanoparticles with Au Core and Nanostructured Pt Shell toward Highly Active Electrocatalysts. *Chem. Mater.* **2010**, *22*, 6310−6318.
(40) Cui, Q.; Shen, G.; Yan, X.; Li, L.; Möhwald, H.; Bargheer, M. Fabrication of Au@Pt Multibranched Nanoparticles and Their Application to In Situ SERS Monitoring. *ACS Appl. Mater. Interfaces* **2014**, *6*, 17075−17081.
(41) Laing, S.; Hernandez-Santana, A.; Sassmannshausen, J.; Asquith, D. L.; McInnes, I. B.; Faulds, K.; Graham, D. Quantitative Detection of Human Tumor Necrosis Factor α by a Resonance Raman Enzyme-Linked Immunosorbent Assay. *Anal. Chem.* **2011**, *83*, 297−302.
(42) Li, J.; Lv, L.; Zhang, G.; Zhou, X.; Shen, A.; Hu, J. Core-Shell Fructus Broussonetia-Like Au@Ag@Pt Nanoparticles as Highly Efficient Peroxidase Mimetics for Supersensitive Resonance-Enhanced Raman Sensing. *Anal. Methods* **2016**, *8*, 2097−2105.
(43) Tokonami, S.; Morita, N.; Takasaki, K.; Toshima, N. Novel Synthesis, Structure, and Oxidation Catalysis of Ag/Au Bimetallic Nanoparticles. *J. Phys. Chem. C* **2010**, *114*, 10336−10341.
(44) Toshima, N.; Ito, R.; Matsushita, T.; Shiraishi, Y. Trimetallic Nanoparticles Having a Au-Core Structure. *Catal. Today* **2007**, *122*, 239−244.
(45) Guo, X.; Zhang, Q.; Sun, Y.; Zhao, Q.; Yang, J. Lateral Etching of Core−Shell Au@Metal Nanorods to Metal-Tipped Au Nanorods with Improved Catalytic Activity. *ACS Nano* **2012**, *6*, 1165−1175.
(46) Petkov, V.; Wanjala, B. N.; Loukrakpam, R.; Luo, J.; Yang, L.; Zhong, C.-J.; Shastri, S. Pt−Au Alloying at the Nanoscale. *Nano Lett.* **2012**, *12*, 4289−4299.
(47) Chou, T. S.; Perlman, M. L.; Watson, R. E. Electronegativity and Electron Binding in Gold Alloys. *Phys. Rev. B: Solid State* **1976**, *14*, 3248−3250.
(48) Demirci, U. B. Theoretical Means for Searching Bimetallic Alloys as Anode Electrocatalysts for Direct Liquid-Feed Fuel Cells. *J. Power Sources* **2007**, *173*, 11−18.
(49) Tian, W. Q.; Ge, M.; Gu, F.; Yamada, T.; Aoki, Y. Binary Clusters AuPt and Au_6Pt: Structure and Reactivity within Density Functional Theory. *J. Phys. Chem. A* **2006**, *110*, 6285−6293.

DOI: 10.1021/acsami.7b17945
ACS Appl. Mater. Interfaces 2018, 10, 12954−12959